Transformer and Line Energisation via Grid Forming Converter based on Multi-Loop Droop Control

Jinsheng Peng, Geoff Love and Zia Emin

***Abstract*--Grid forming converters are expected to become the main voltage source for electrical power systems in future grids, as many of the conventional power plants based on synchronous generators are being replaced by renewable generating plants interfacing with grids via converters. This paper evaluates network energisation via grid forming converter based on multi-loop droop control, focusing on transformer inrush and switching overvoltages. The evaluation utilizes simulation conducted in PSCAD-EMTDC to investigate the scenarios of using a 50 MVA battery energy storage plant with grid forming converters to sequentially energise part of a 132 kV network. The results are analysed and compared with those obtained under the scenario of energising the same network via a 50 MVA synchronous generator. The studies serve to identify the potential differences between grid forming converters and synchronous generators in terms of their impacts on transformer inrush transients and cable switching overvoltages. In addition, the influences of grid forming converter aggregation, controller parameter settings and current limiter settings on the inrush and switching transients are investigated.**

***Keywords*: Energisation Transient, Grid Forming Converter, Overvoltages, Synchronous Generator, Transformer Inrush.**

I. Introduction

In many countries, there is a transition from synchronous generators (SG) powered by conventional sources (such as coal, oil and gas) to wind and solar power renewable generation. This is one of the key solutions to combatting climate change. An important part of this transition is the use of grid forming converter (GFM) which are being considered as an essential component in future grids regulation of system voltage and frequency, and to maintain system stability. The transition to a GFM dominated power grid requires research and testing on GFM's capabilities, in terms of system steady state operation, inertia and short circuit current contribution, dynamic stability, power quality and electromagnetic transients under network switching and energisation.

Network energization, as part of network restoration involves the energizing system of components including transformers, transmission circuits, shunt compensation equipment and loads (including large motors). Conventionally, synchronous generators have been the main voltage sources for supplying the transient current and overvoltages incurred by network energisation transients such as transformer inrush, resonant overvoltages and switching overvoltages. Recently, a number of research and industrial projects have been carried out to assess network energisation transients under the scenarios of using GFMs to black start power system networks [1-4], as it is envisaged that the GFMs will be tasked to provide services for network restoration. For power systems of remote islands and microgrids, an increasing number of projects are demonstrating the feasibility of utilising a combination of GFM-based wind, solar and battery storage plants in black starting and maintaining supply to an island system. An example consists of a 5.2 MVA of battery storage and 3.85 MVA of solar to supply an electrical grid with a peak demand of about 2 MW [2]. At transmission and distribution grid, ancillary service projects have been carried out: such as Resilience as a Service project which investigates transformer inrush transients under the scenario of using a 5 MVA rated battery storage to energise part of distribution network [3]. The Distributed ReStart project explored black start from distributed energy resources, where live trials of GFMs to energise part of transmission network were performed. This included a case of energising a 240 MVA transformer via a wind farm consisting of four units of 3 MW GFM [4]. In other areas, modelling and simulations of using GFM as a black-start source for energising inductive motor loads of a generating plant were evaluated in [5]. Black start from a PV-battery plant was investigated in [6] and black start from HVDC-connected offshore wind farm was studied in [7].

Among many of the projects, both soft-start approach and direct-on-line energisation method were considered. Although the soft-start approach could reduce inrush current and overvoltage issues [8-10], it has implications on system protection which could result in no identification or selectivity for some critical faults, and it may not be applicable to the network with existing loads connected. Therefore, there are incentives to evaluate the scenario of direct-on-line energisation to assess the voltage and current transients and to verify whether there are sufficient margins for GFM(s) and system equipment to accommodate and withstand the transients.

This paper aims to investigate direct-on-line energisation of transmission network via GFM, with a focus on assessing inrush transients due to transformer energisation and switching overvoltages due to energisation of cable circuit. The evaluation was carried out based on simulation conducted in PSCAD-EMTDC to investigate the scenario of using a 50 MVA battery storage plant with GFMs to sequentially

Jinsheng Peng was with Power System Consulting (PSC), Warwick UK. He later joined Ørsted UK (e-mail: jinpe@orsted.com)

Zia Emin is with Power System Consulting (PSC), Warwick UK (e-mail of corresponding author: zia.emin@pscconsulting.com).

Geoff Love is with Electric Power Research Institute (EPRI), Dublin IRL (e-mail: glove@epri.com).

Paper submitted to the International Conference on Power Systems Transients (IPST2023) in Thessaloniki, Greece, June 12-15, 2023.

energise part of a typical 132 kV transmission network. The results were comparatively analysed with those obtained by energising the network via a 50 MVA SG to identify the differences between GFM and SG on network energisation transient. The studies contribute to demonstrate the potential advantages of GFM compared to SG in terms of reducing inrush currents during transformer energisation and leading to less severe switching overvoltages upon cable energisation. The evaluation also investigated the potential impacts of GFM aggregation approach and the influences of GFM's controller and current limiter settings on the transient study results.

II. Network under Study

Network under study consists of a voltage source capable for black starting part of the transmission network that includes a 13.8/132 kV main transformer connecting to a 132 kV cable circuit (as shown in Fig. 2). The circuit is aimed to represent a typical part of transmission network required to be energized at the initial stage of network restoration process.

Two types of voltage sources are considered in this study, one based on SG and the other based on GFM. The voltage source is considered to be generator with a relatively large MVA rating connected to a transmission network. In this case, a SG is normally with a terminal voltage at medium voltage (MV) level and directly connected to a MV busbar. In contrast, with relatively small MVA size compared to SG, a number of GFM converters are required to form a battery storage plant (or renewable generating plant) with a MVA rating compatible to that of a SG-based power plant. The terminal voltage of GFM is normally at low voltage (LV) level (less than 1 kV) and therefore usually require a unit transformer for stepping up voltage from LV to MV.

The SG-based voltage source corresponds to a hydro power plant which is assumed installed with a 50 MVA SG with a rated terminal voltage of 13.8 kV. The schematic of the SG-based voltage source is shown in Fig. 2a. The SG is controlled by automatic voltage regulator (AVR) and a governor connected to a hydro turbine. A hydro power plant has been chosen due to its favourable characteristics as black start resource. These characteristics include fast restart, adequate on-site fuel supply, large real and reactive power capacity, ability to operate during frequency excursions and ability to stabilise system frequency and support voltage [11].

The GFM-based voltage source corresponds to battery energy storage system (BESS). A BESS plant as a black start source has capability to self-start. Furthermore, it has rapid control of voltage and frequency and can be set with grid forming characteristics for network energisation. However, consideration should be given to maintaining a suitable level of state of charge and the limitation that the stored energy in a BESS can only provide power for a time limited period (e.g., over several hours). The BESS plant consists of five units of 10 MVA GFMs. The schematic of the detail representation of the BESS plant is as shown in Fig. 2b. Each GFM has a terminal voltage of 0.8 kV and is connected to a MV busbar via a 10 MVA (0.8/13.8 kV) unit transformer and a short 50 m length cable. The MV voltage has the same voltage as SG terminal voltage.

In addition, two aggregated representations of the GFM plant are considered, Aggregation-1 (Fig. 2c) and Aggregation-2 (Fig. 2d). GFM Aggregation-1 (GFM-A1) aggregates at the MV level, and is a single 50 MVA GFM, connected directly at the 13.8 kV bus. GFM-A1 corresponds to a direct-MV-connect-converter which is currently rare but may become common in the future. GFM Aggregation-2 (GFM-A2) is also a 50 MVA aggregation, but it is connected at the 0.8 kV LV bus and includes an aggregated 50 MVA (0.8/13.8 kV) unit transformer and an aggregated MV cable feeder. The aggregated unit transformer is modelled with the short-circuit impedance and the magnetizing reactance reduced to one fifth of the nominal values of the 10 MVA unit transformer used in Fig. 2b. Similarly, the aggregated cable circuit is modelled with the impedance reduced to one fifth of the nominal values of the MV cable, but with the capacitance value increased by a factor of five.

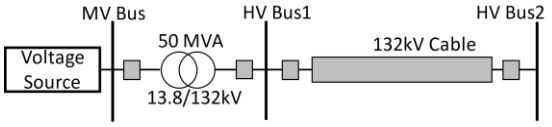

Fig. 1. Schematic of network under study

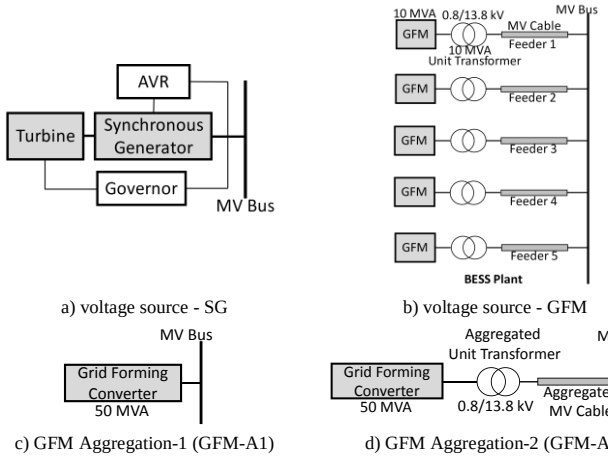

Fig. 2. Schematic of voltage source representation

III. Network Modelling

This section presents the approach utilised for modelling GFM, SG, transformers and cable circuit.

A. GFM Model

Various type of GFM control algorithms have been proposed in literature. This paper focuses on the GFMs based on the multi-loop droop control scheme. The GFM model is based on that implemented in the open-source PSCAD grid forming inverter model developed by NREL [12]. As shown in Fig. 3, the GFM model consists of controlled voltage sources (one on each phase) connected to grid side busbar via a LCL filter. The GFM controller is based on the multi-loop droop control strategy, having a cascaded structure including the outer P-f droop control, outer voltage regulator, inner voltage control loop and inner current control loop. As demonstrated in [13], the target voltage of the multi-loop droop control is the inverter filter capacitor voltage.

The outer active power droop control and the voltage regulator control is shown in Fig. 4a. The active power droop control sets and adjusts the angular frequency ω. The integration of the frequency produces the phase angle θ which ramps from 0 to 2π and is the angle used in Clarke and Park transformations. The outer voltage regulator is based on a closed loop voltage regulation using a PI controller to control the magnitude of the filter capacitor voltage.

The inner voltage and current loops (as shown in Fig. 4b and Fig. 4c) are utilised to achieve fast control of the filter capacitor voltage v_o and the converter current i_f. Both control loops utilise PI controller with decoupling of *dq*-frame components. Based on the voltage reference from the output voltage regulator, the voltage loop controls the filter capacitor voltages v_{od} and v_{oq} via the PI controller with the proportional gain k_{pv} and the integral gain k_{iv}. The output current i_o is applied to the controller via the current feed forward gain G_V. The outputs of the voltage control loop are applied as the current references for the current control loop. The current loop controls the converter output currents i_{ld} and i_{lq} via the PI controller with the proportional gain k_{pi} and the integral gain k_{ii}. The filter capacitor voltages (v_{od} and v_{oq}) are applied to the controller via the voltage feed forward gain G_C. The outputs of the current control loop are voltages in *dq*-frame for control of the voltage source. The controller parameter settings used in the studies are those provided in [12].

A current limiter (with an aim to limit the converter current i_f) is implemented between the inner control loops (as shown in Fig. 4b) to apply restriction to the current references when it is detected that the magnitude of the current order from the inner voltage control loop is larger than the current limit (I_{max}). The logic and the associated schematic of the current limiting function are as shown in Fig. 5. When the magnitude of the current I_{dq} is larger than the current limit (here a default limit of 1.1 pu is used), both the *d*- and *q*-axis current references associated are scaled down by multiplying the I_{dq_scale}. The current limiter only decreases the magnitude of the original current reference. The angle of the current reference remains the same under the current limiting.

A. SG Model

The SG model was set up to represent a 50 MVA machine installed in a hydro generating plant. The model consists of a salient pole synchronous machine, the associated exciter and the turbine-governor. The synchronous machine is represented based on the PSCAD library model which considers the machine armature resistance, the leakage reactances (including steady state, transient and sub-transient reactances) and the associated time constants. The D-axis saturation is considered in the model.

The AVR applied to the machine is the AC1A model of an AC rotating exciter. The governor model uses the IEEE type Gov-1 to represent the mechanical-hydraulic controls. The turbine is based on the IEEE type TUR1 for representing the hydro turbine with non-elastic water column with a surge tank.

B. Transformer Model

The transformers are three-phase two-winding transformer assumed with three-limb core structure, which are represented utilising the duality-based multi-limb transformer model with normalized core concept as presented in [14]. The model considers core topology by direct application of the principle of duality by placing electric components on the geometry of the transformer core. The model accounts for the effects of saturation in each individual leg of the core as well as the interphase magnetic coupling. The saturation characteristic of core inductance is represented based on the assumptions that the nominal magnetic flux density of transformer core is of 1.7 Tesla and the air-core reactance is two times of the transformer positive-sequence leakage reactance. The transformer magnetisation branch is modelled with Jiles-Atherton (JA) hysteresis based on PSCAD'S default settings.

C. Cable Circuit Model

The cable circuit is of 132 kV single-core land cable with copper conductor (630 mm^2), XLPE insulation, copper wire sheath and polypropylene outer jacket. The three single-core cables for the cable circuit are laid underground in open trefoil. The details of cable dimensions and the cross-bonding of the cable system are based on those provided in [15]. Each single-core cable is modelled in PSCAD based on the Frequency Dependent (Phase) Model, utilising the four-layer representation covering conductor, insulation, metallic sheath and outer cover layers.

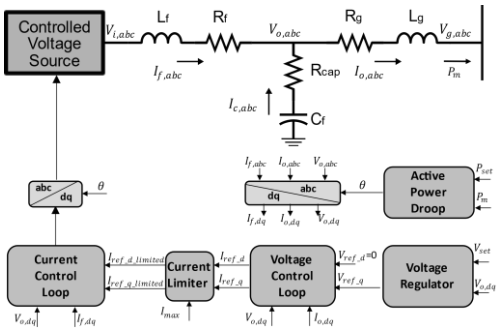

Fig. 3. Schematic of GFM circuit and controller structure

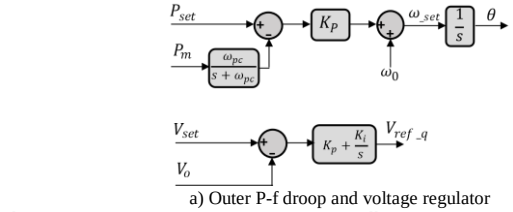
a) Outer P-f droop and voltage regulator

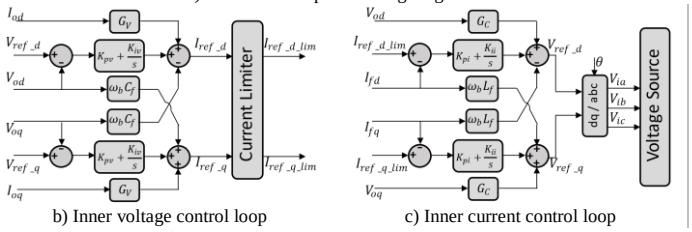

b) Inner voltage control loop c) Inner current control loop

Fig. 4. Schematic of GFM outer and inner control loops

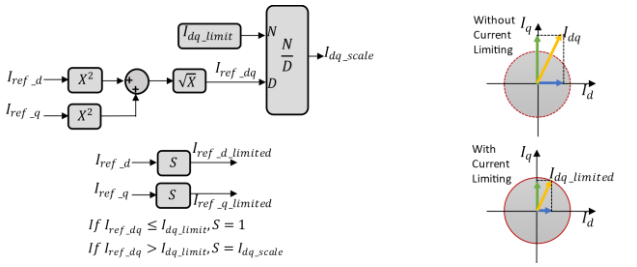

a) Current limiter logic b) Schematic of limiting

Fig. 5. GFM current limiter logic and schematic of limiting function

IV. Transformer Energisation Study

When a magnetic-core based transformer is energised against a voltage source, the voltage applied to the transformer causes build-up of flux linkage which can saturate the transformer core and lead to large inrush currents. It is well known that the magnitude of the inrush currents is mainly influenced by the point-on-voltage-wave switching angles, the residual flux and the saturation inductance of the transformer core. The decay of the inrush currents is mainly determined by the resistive element of the circuit between the voltage source and the transformer winding being energised. If there are any transformers already connected in series or in parallel with the transformer to be energised, sympathetic interaction can occur between the transformers. This occurs because the inrush currents are drawn by the incoming transformer flowing through the system resistance can make the system voltages become asymmetrical and saturate the already connected transformers [16]. The sympathetic interaction can significantly prolong the duration of transformer inrush transient, and potentially lead to temporary harmonic overvoltage if the system has low order harmonic resonances.

Based on the network under study, the inrush transients due to energising the 50 MVA main transformer is assessed with the simulation cases listed in Table I. The first case set (SG-ENT) energises the transformer via a hydro-power plant installed with a 50 MVA synchronous generator. The second case set (GFM-ENT) energises the transformer via a GFM-based BESS plant consisting of five units of 10 MVA GFM and the associated MV transformers and cable feeders. Zero and maximum residual flux conditions were considered for each network. The maximum residual flux is assumed with a distribution of 80%, 0% and -80% residual flux at phase-A, B and C respectively. In addition, case set (GFM-A1-ENT) simulates energisation of the transformer based on the model with GFM-A1. Case set (GFM-A2-ENT) considers utilising GFM-A2.

For all the cases, a systematic switching study is conducted to cover the energisation angles evenly distributed over one power frequency cycle. In the simulation, the selected step for the switching angle variation is 6 degrees, which results in a total of 60 runs carried out over one fundamental frequency cycle. At each switching angle, the three phase closing times are assumed to be the same (i.e., simultaneously closed at the same point-on-voltage-wave switching angle).

TABLE I
List of Baseline Study Cases

Case Name	Voltage Source	Switching Angle	Residual Flux
SG-ENT-1	Synchronous Generator	0–360 degrees	Zero
SG-ENT-2			Maximum
GFM-ENT-1	GFM with detailed representation	0–360 degrees	Zero
GFM-ENT-2			Maximum
GFM-A1-ENT-1	GFM-A1	0–360 degrees	Zero
GFM-A1-ENT-2			Maximum
GFM-A2-ENT-1	GFM-A2	0–360 degrees	Zero
GFM-A2-ENT-2			Maximum

A. Energisation with Zero Residual Flux (ENT-1)

The set of ENT-1 study energises the 50 MVA main transformer assuming that there is zero residual flux in the transformer core. The variation of inrush current peak magnitudes (maximum out of three phases) and GFM current limiter status against the switching angles are compared in Fig. 6 (the zero degree corresponds to the positive-going zero-crossing of phase-A to ground voltage). The peak magnitudes are based on per unit values of the main transformer's peak full load current at the 13.8 kV side.

The result of energising the transformer against an ideal voltage source (shown in black curve) is included as the baseline for comparison. The inrush current magnitudes produced under the SG and GFM cases are much smaller than those of the ideal voltage source case, indicating that the voltage drop across the internal impedance of SG and GFM contribute to significant reduction of the peak magnitudes.

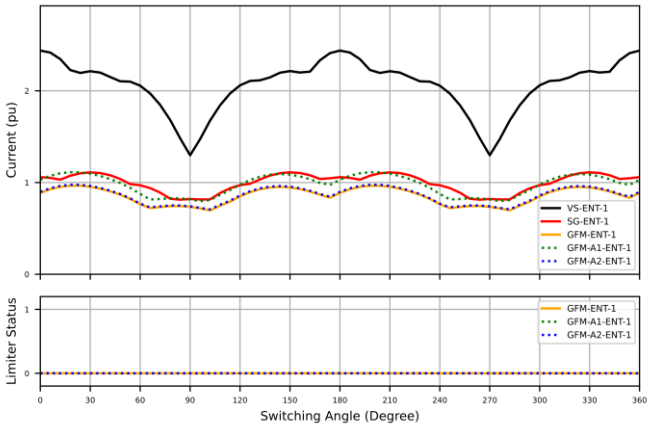

Fig. 6. Energisation cases with zero residual flux (study set ENT-1) - Variation of inrush current peaks (upper plot) and GFM current limiter status (lower plot) against point-on-voltage-wave switching angle

In all cases a pattern can be seen in that the inrush current peaks in the first half cycle repeat in the second half cycle). In the case of GFM-A1-ENT-1 (where the GFM units are aggregated to MV busbar), the maximum peaks are in the same order as those produced by energising against SG. In the other two GFM cases (GFM-ENT-1 and GFM-A2-ENT-1), the produced current peaks are slightly lower, as the impedances of the MV transformers and cable feeders contribute to the reduction of the inrush current peaks. The comparison between the GFM cases demonstrates that the aggregated model taking account of the MV network (GFM-

A2) can produce results that are identical with those generated by the model with distributed representation of the GFM units and the MV feeders. However, there are some differences when the GFM is aggregated at the MV network (GFM-A1).

In all the examined GFM cases associated with the study set ENT-1, no triggering of GFM current limiter was identified for any of the evaluated switching angles. The inrush current did not breach the 1.1 pu overload rating used in the GFM controller's inner loop current limiter.

For the energisation conducted at the zero-crossing of MV phase-A to ground voltage, the time domain inrush currents at the MV side of the main transformer are plotted in Fig. 7. This figure shows that the inrush currents produced when energising against an SG have a slower initial decay (when comparing first and second current peaks) than when energising against a GFM. The GFM has a faster voltage control loop that helps to control the voltages in such a way that it reduces the build-up of asymmetrical flux-linkage in the transformer core under inrush transient. This is evident in the comparison between GFM-A1 (MV-connected converter) and SG regarding the phase-A voltage (shown in Fig. 8). However, in the GFM cases with an MV unit transformer(s), it is found that the fast voltage control can cause saturation of the MV transformers which leads to series sympathetic interaction between the unit transformer and the main transformer, resulting in a prolonged inrush current decay (as shown in the inrush currents of the GFM-Detailed and the GFM-A2 cases, which are identical to each other).

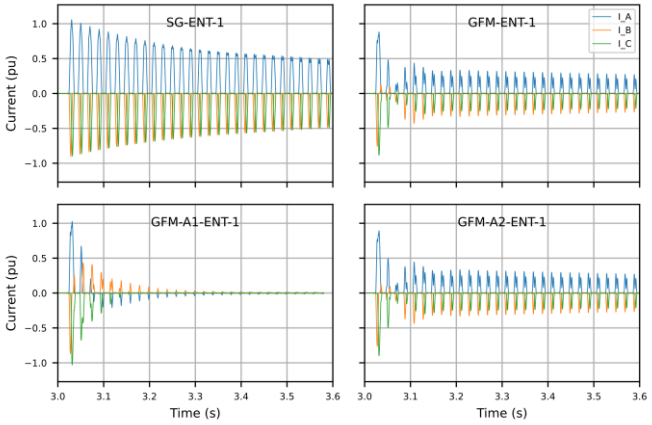

Fig. 7. Energisation cases with zero residual flux – Inrush currents at the LV side of main transformer resulted from energisation conducted at positive-going zero-crossing of phase-A to ground voltage of MV busbar

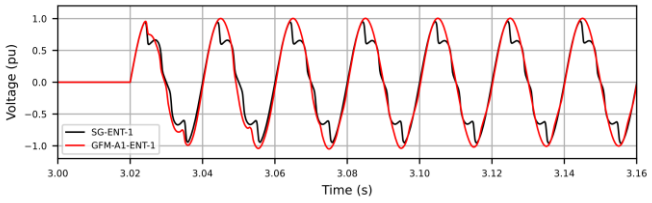

Fig. 8. Energisation cases with zero residual flux – Phase-A voltage at the LV side of main transformer resulted from energisation at voltage zero-crossing

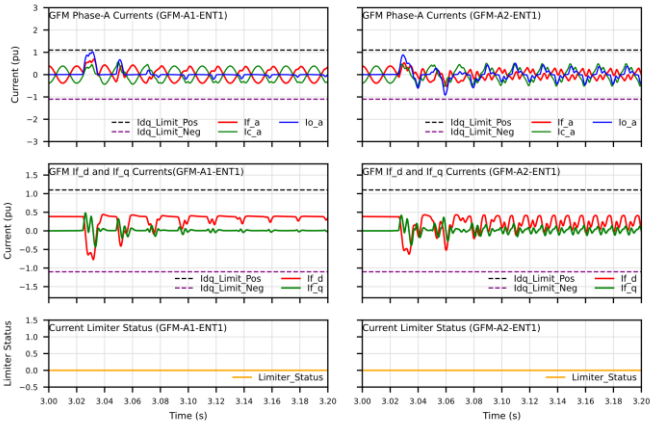

Fig. 9. Time domain GFM currents and limiter status resulted from energisation conducted at zero-crossing of phase-A with zero residual flux in main transformer (left plots are for GFM-A1, right plots for GFM-A2)

The time domain GFM currents (taking phase-A currents as example) are shown in Fig. 9 for the case GFM-A1-ENT-1 and GFM-A2-ENT-1. Under the initial steady state no-load condition, the GFM output current i_f (flowing through the filter inductor) is primarily supplying the filter capacitor charging current i_c (the charging current is of 0.4 pu for the selected size of filter capacitor). The summation of the two currents (i_f and i_c) forms the GFM current i_o injected to the grid, which is of negligible level prior to energisation. Upon transformer energisation, both the GFM and the filter capacitor contribute to supply the inrush current caused by transformer saturation. A rapid reduction of inrush current is seen in the GFM-A1 case, while a prolonged inrush current is supplied in the GFM-A2 case due to the series sympathetic interaction between the unit transformers and the main transformer. The unit transformers also cause 30˚ phase shift and result in inrush current waveshape different from that of GFM-A1. In both cases, the *dq*-components of the current i_f are below the 1.1 pu current limit and therefore there is no activation of GFM current limiter.

B. Energisation with Maximum Residual Flux (ENT-2)

The set of ENT-2 study cases consider energising the main transformer assuming that there is maximum residual flux in the core. The variation of inrush current peak magnitudes (maximum out of three phases) and GFM current limiter status against the switching angles are shown in Fig. 10. The black curve is associated with energising the transformer against ideal voltage source which as expected produces a much higher inrush currents than the SG and GFM cases.

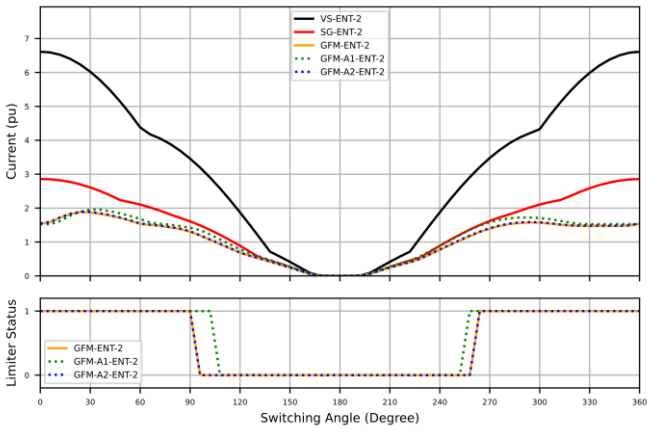

Fig. 10. Energisation cases with maximum residual flux (study set ENT-2) – Variation of inrush current peaks (upper plot) and GFM current limiter status (lower plot) against point-on-voltage-wave switching angle

For the ideal voltage source and SG cases, the patterns exhibit a mirror image between the first and the second half cycle. The maximum inrush current peaks were identified at the positive-going zero-crossing of phase-A voltage (referred to 0˚ in Fig. 10) where the energisation results in maximum positive build-up of flux linkages on top of the residual flux. At the energisation angle of negative-going zero-crossing of phase-A voltage (180˚), inrush current is eliminated as the applied voltages would generate flux linkages are in line with the prospective flux linkages (this is also the target angle for controlled switching). For the GFM cases, the inrush current peaks are lower than the SG case. The patterns were identified to be asymmetry between the first and the second half cycle and the maximum peaks were identified at the switching angles around 30˚. This was found mainly due to the reasons that the GFM output current i_f is influenced by the GFM current limiter and that the filter capacitor current i_c is varied by the filter capacitor voltage during inrush transient. The variation of both currents (i_f and i_c) has an impact on the total GFM current i_o injected to the grid. The results of current limiter status (shown at the lower plot of Fig. 10) demonstrate that the current limiter can triggered for a wide range of switching angles under maximum residual flux scenario.

For the energisation conducted at the positive-going zero-crossing of MV phase-A to ground voltage, the time domain inrush currents at the MV side of the main transformer are compared in Fig. 11. It is evident that in the GFM cases, the produced inrush currents are of much smaller magnitude than that of the SGT case. For this case, in addition to GFM's fast voltage control (as evident in Fig. 12), the current limiter within the GFM controller plays a significant role in reducing the inrush current peaks. Similar to the scenario with zero residual flux, a rapid decay of inrush current is seen in the GFM-A1 case (without MV network). In the other GFM cases (GFM-Detailed and GFM-A2) involving the MV transformers, the inrush currents are prolonged by the series sympathetic interaction between the unit transformer and the main transformer. The results suggest that, for the GFM plants consisting of unit transformers connected between the GFM(s) and the main transformer to be energised, the GFM-A2 is a more realistic and accurate aggregation approach than GFM-A1, as it can adequately take account of sympathetic interaction between the unit transformer(s) and the main transformer.

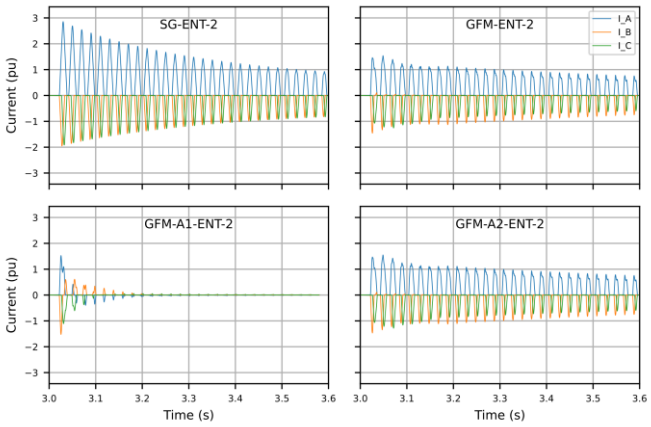

Fig. 11. Energisation cases with maximum residual flux – Inrush currents at the LV side of main transformer resulted from energisation conducted at positive-going zero-crossing of phase A to ground voltage of MV busbar

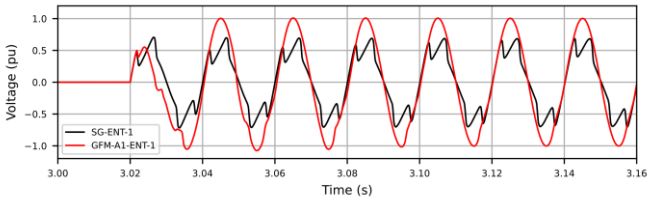

Fig. 12. Energisation cases with maximum residual flux – Phase-A voltage at the LV side of main transformer due to energisation at voltage zero-crossing

The time domain GFM currents for the cases GFM-A1-ENT-2 and GFM-A2-ENT-2 are shown in Fig. 13 which includes the phase-A currents, *dq*-frame components of i_f and current limiting status. Upon energisation, in the GFM-A1 case, the current limiter was triggered to limit the first peak of the inrush current, while in the GFM-A2 case, the current limiter was triggered multiple times over a period of the first 140 ms. The number of current limiter activation is an indicator of the potential level of thermal stresses on the converter's power electronic devices. The current limiter was restricting the dq-frame components of the GFM output current i_f to be within the 1.1 pu limit which is shown by the dash lines in Fig. 13. Note that, although the GFM output current i_f is limited, the total current injected to grid (i_o) can exceed the current limit when it is added with the filter capacitor current (i_c).

Although not shown in this paper, it was identified that the GFM's controller parameters can influence the inrush currents. Increasing the PI gains of the inner control loop (either the current loop or the voltage loop) can lead to increase of inrush current magnitudes. Decreasing the PI gains would reduce the inrush current peaks. In addition, reducing the current limiter setting can reduce the inrush current peaks.

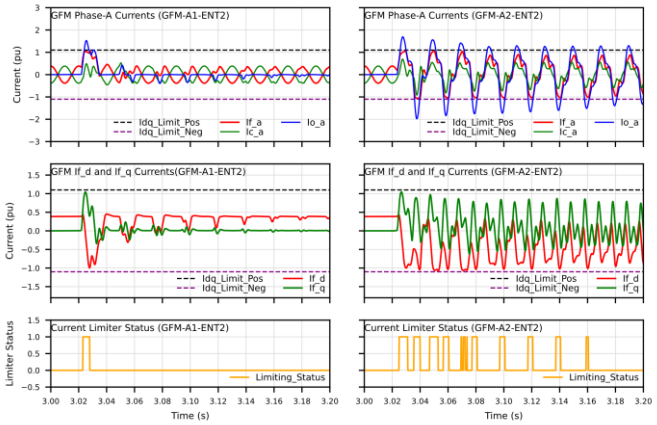

Fig. 13. Time domain GFM currents and limiter status resulted from energisation conducted at voltage zero-crossing with maximum residual flux in main transformer (left plots are for GFM-A1, right plots for GFM-A2)

V. Cable Energisation

A statistical switching study was conducted to evaluate transient overvoltages due to energisation of the 132 kV cable. For simulation of statistical switching, 200 instances of closing time were generated in accordance with the approach suggested in the IEC TR 60071-4:2004 [17]. The closing command was assumed to be uniformly distributed over one power-frequency cycle and the closing times of the three phases were set to be around the closing command following Gaussian distribution with a standard deviation of 1 ms.

The maximum peaks (out of three phases) of the calculated phase-to-ground overvoltages are compared between SG and GFM energisation cases (as shown in Fig. 14) in terms of the cumulative probability distribution of overvoltages. For one of the worst energisation cases, the time domain phase-to-ground voltages are shown in Fig. 15 for comparison between the SG case and the GFM case with detailed representation of GFMs.

In the comparison between SG and GFM cases, the results suggest that energising the cable via SG is shown to cause higher overvoltages than energising via GFM. The results of the overvoltages calculated based on the aggregated representation of the GFM plant are largely similar with those produced based on the detailed representation. However, the GFM-A1 (simplified aggregation without considering the MV network) can result in lower values being calculated for the maximum top 10% overvoltages. The lower overvoltages in the GFM cases can be ascribed to GFM's fast inner control loops that help to suppress the excursion of the initial transient overvoltages. This is also evident in the time domain plot in Fig. 15 which shows that the energisation via GFM causes lower first peak and has faster decay of the overvoltage transients than that of the SG cases.

The sensitivity of the cable switching overvoltages to the GFM's current limiter and control loop settings was also studied (but not shown here). It was identified that the overvoltages can potentially be reduced by lowering the current limit or the PI gains of the inner control loops.

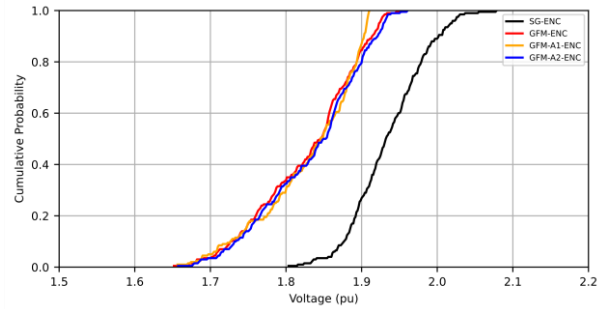

Fig. 14. Cumulative probability distribution of maximum voltage peaks

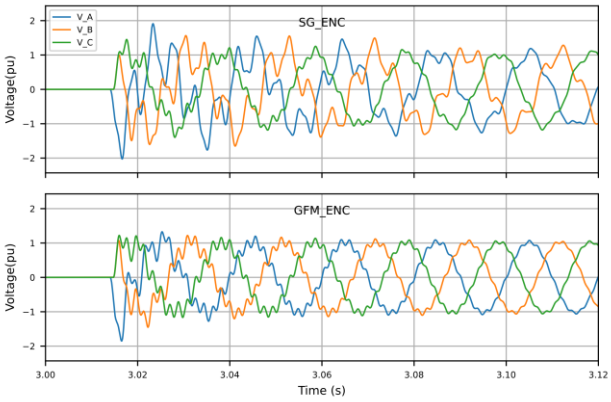

Fig. 15. Time-domain phase-to-ground voltages due to cable energisation (comparison between SG-ENC and GFM-ENC)

VI. Conclusions

This paper evaluates network energisation via GFM based on multi-loop droop control, with focus on transformer energisation and cable switching transients. The scenarios of using a 50 MVA GFM-based battery energy storage plant to energise part of a 132 kV transmission network were investigated based on a series of systematic and statistical simulation studies conducted in PSCAD-EMTDC. The results have been analysed and compared with those obtained under the scenario of energising the same network via a 50 MVA SG-based hydro generating plant. The studies have identified the potential differences between GFM and SG in terms of their impacts on transformer inrush transients and cable switching overvoltages.

With regard to transformer energisation, it is demonstrated that the inrush currents produced by energising against GFM are with lower magnitude and faster initial decay than energising against SG, as the GFM has current limiter to restrict inrush current peak magnitudes and has fast voltage control loop that helps to reduce the build-up of asymmetrical flux-linkage in the transformer core. However, it is identified that a prolonged transformer inrush can appear in the GFM plant with unit transformer(s) connected in series with the main transformer to be energised. This suggests that it is important to include the GFM's unit transformer(s) in detailed or aggregated representation of GFM plant to adequately take account of potential sympathetic interaction.

For switching overvoltages due to cable energisation, it is identified that energising the cable via GFM is likely to cause less severe overvoltages than energising via SG.

VII. REFERENCES

[1] National Grid ESO, "Black Start from Non-Traditional Generation Technologies", July 2019.

[2] O. Schomann, "Experiences With Large Grid-Forming Inverters on Various Island and Microgrid Projects," in 4th International Hybrid Power Systems Workshop, Crete, Greece, May 2019.

[3] D. Vozikis and A. Emhemed, "Modelling and Simulation Studies of Inrush Current Phenomena Associated with the Application of RaaS – Drynoch Distribution Network", technical report by WSP, July 2021.

[4] Distributed ReStart, "Demonstration of Black Start from DERs (Live Trials Report) Part 1", December 2021.

[5] H. Jain, G.-S. Seo, E. Lockhart, V. Gevorgian, and B. Kroposki, "Blackstart of power grids with inverter-based resources," in Proc. IEEE Power Energy Soc. Gen. Meeting (PESGM), Aug. 2020, pp. 1–5.

[6] Q. Nguyen, M. R. Vallem, B. Vyakaranam, A. Tbaileh, X. Ke, and N. Samaan, "Control and Simulation of a Grid-Forming Inverter for Hybrid PV-Battery Plants in Power System Black Start", in IEEE Power & Energy Society General Meeting (PESGM), July 2021.

[7] A. Jain, O. Saborío-romano, J. N. Sakamuri, and N. A. Cutululis, "Blackstart from HVDC-connected offshore wind: Hard versus soft energization", IET Renewable Power Generation, vol. 15, no. 1, pp. 127-138, 2021.

[8] S. Cherevatskiy, S. Sproul, S. Zabihi, R. Korte, H. Klingenberg, B. Buchholz, and A. Oudalov, "Grid forming energy storage system addresses challenges of grids with high penetration of renewables (A case study)", CIGRE Session 48, C2-C6-322, Paris, August 2020.

[9] Energy Systems Integration Group's High Share of Inverter-Based Generation Task Force (2022, Mar.). Grid-Forming Technology in Energy Systems Integration. Available: https://www.esig.energy/wp-content/uploads/2022/03/ESIG-GFM-report-2022.pdf

[10] A. Alassi, K. Ahmed, A. Egea-Alvarez, and C. Foote, "Modified grid-forming converter control for black-start and grid-synchronization applications", in 2021 UPEC Conference, 31 Aug.-3 Sept. 2021, pp. 1-5

[11] Gracia, J. R., L. C. Markel, D. T. Rizy, P. W. O'Connor, R. Shan, and A. Tarditi, "Hydropower Plants as Black Start Resources", Oak Ridge National Laboratory, May 2019.

[12] R. W. Kenyon, A. Sajadi, A. Hoke, and B.-M. Hodge, "Open-source pscad grid-following and grid-forming inverters and a benchmark for zero-inertia power system simulations," in 2021 IEEE Kansas Power and Energy Conference (KPEC), 2021, pp. 1–6.

[13] W. Du, Z. Chen, K. P. Schneider, R. H. Lasseter, S. Pushpak, F. K. Tuffner, and S. Kundu, "A comparative study of two widely used grid-forming droop controls on microgrid small signal stability," pp. 1-1.

[14] M. Shafieipour, J. C. Garcia A., R. P. Jayasinghe, and A. M. Gole, "Principle of Duality with Normalized Core Concept for Modeling Multi-Limb Transformers," International Conference on Power Systems Transients (IPST), Perpignan, France, Jun. 17-20, 2019, pp. 1-6.

[15] M. Z. Daud, P. Ciufo, and S. Perera, "Investigation on the suitability of PSCAD/EMTDC models to study energisation transients of 132kV underground cable", in Australasian Power Engineering Conference, Sydney, Australia, Dec 2008.

[16] H. Bronzeado and R. Yacamini, "Phenomenon of sympathetic interaction between transformers caused by inrush transients," IEE Proceedings - Science, Measurement and Technology, vol. 142, no. 4, pp. 323-329, 1995.

[17] Insulation co-ordination – Part 4: Computational guide to insulation co-ordination, IEC TR 60071-4:2004, Jun. 2004.